Available online at www.sciencedirect.com
ScienceDirect
Earth and Planetary Science Letters 260 (2007) 137–151
EPSL
www.elsevier.com/locate/epsl

Controls of conduit geometry and wallrock elasticity on lava dome eruptions

A. Costa [a,c,*], O. Melnik [a,b], R.S.J. Sparks [a]

[a] Centre for Environmental and Geophysical Flows, Department of Earth Sciences, University of Bristol, Bristol, UK
[b] Institute of Mechanics, Moscow State University, Moscow, Russia
[c] Istituto Nazionale di Geofisica e Vulcanologia, Naples, Italy

Received 25 July 2006; received in revised form 19 December 2006; accepted 2 May 2007
Available online 23 May 2007
Editor: C.P. Jaupart

Abstract

Many lava dome building eruptions show periodic to complex non-periodic pulsatory activity. Typical time-scales associated with this activity range from hours to decades. Previous studies modelled the ascent of magma using a set of transient 1-D transport equations, accounting for degassing induced crystallization kinetics, gas exsolution and viscosity increase due to crystal growth. These models assumed flow in a cylindrical conduit with a fixed cross-section area. Since several observations suggest that extrusions are mainly fed by dykes, with cylindrical geometries developing only at shallow levels, here we generalised the model to the flow geometry represented by an elliptical dyke with major and minor semi-axes changing with depth. Quasi-static elastic deformation of the dyke is accounted by an analytical solution that couples cross-section area with the magmatic overpressure. The effects of the main dyke geometrical parameters and boundary conditions on the eruption dynamics were investigated. The presence of a deformable dyke can lead to a more complex periodic behaviour with a wider range of time-scales and cyclicity patterns with respect to a uniform cylindrical conduit. There is a regime where the period of pulsations is controlled by the elasticity of the dyke and a regime where the period is controlled by the volume of the magma chamber. Intermediate regimes are possible. Periodic variations in discharge rate are also possible for both fixed pressure in dyke source region and fixed influx rate into the dyke. Our study emphasizes the strong non-linearities and complex behaviours of lava dome eruptions. From a forecasting and hazard perspective, intrinsic uncertainties in governing parameters may make volcanic systems in some circumstances unpredictable. On the other hand, lava dome systems may also develop episodic and systematic behaviours so that behaviour becomes predictable for a while.

Keywords: lava dome; extrusive eruption; dyke; wallrock elasticity; periodic behaviour; numerical model

1. Introduction

Many volcanic phenomena are controlled principally by the transport of magma from depth through conduit systems to the Earth's surface. Recent modelling studies (Melnik and Sparks, 1999; Barmin et al., 1999; Massol et al., 2001; Melnik and Sparks, 2005) together with textural studies (Cashman, 1992, 2004) have established that conduit flows in lava dome eruptions can be highly non-linear due to the complex relationships between magma decompression, degassing, degassing-induced crystallization and rheological properties. Periodic

* Corresponding author. Istituto Nazionale di Geofisica e Vulcanologia, Naples, Italy. Tel.: +39 081 6108 446; fax: +39 081 6108 351.
E-mail address: costa@ov.ingv.it (A. Costa).

0012-821X/$ - see front matter © 2007 Elsevier B.V. All rights reserved.
doi:10.1016/j.epsl.2007.05.024

behaviour can develop in the models as the flow system oscillates between alternative stable states. For models with magma supply from elastic-walled chambers, the volume of the chamber and radius of the conduit are important controls on the periodicity. The models hold promise for explaining the common episodic and sometimes approximately periodic behaviour of lava dome eruptions (Melnik and Sparks, 2005; Dirksen et al., 2006), for interpreting geophysical data (Voight et al., 1999; Sturton and Neuberg, 2006; Green and Neuberg, 2006), and accounting for some petrological features of the magmas, which reflect decompression and pressure fluctuations recorded in mineral assemblages, mineral compositions and textures (Cashman, 1992, 2004).

The conduit system plays a key role in terms of both mechanics and fluid dynamics of the flow processes. Much of the work hitherto on volcanic conduit flows has focussed on the fluid dynamics with relatively simple geometries and mechanical behaviours. For lava dome eruptions the models have treated the conduit as a cylinder and do not take into account the elasticity of the wallrocks. The behaviour of magma-filled fractures (dykes) that feed growing lava domes has not been fully investigated.

This study investigates the role of dykes as conduits for lava dome eruptions building on previous research on the non-linear dynamics of dome extrusions (Melnik and Sparks, 1999; Barmin et al., 1999; Melnik and Sparks, 2005). These modelling studies have treated the conduit as a cylinder and have only considered the elastic deformation of the magma chamber supplying the conduit. In this case the geometry allows elastic deformations to be neglected because the large rigidity of rocks means that variations in the radius are very small for large pressure variations. However, elastic deformation cannot be neglected in a dyke geometry. Elastic deformation of dyke walls due to variations in magma pressure results in large changes in dyke width (e.g., Lister and Kerr, 1991; Rubin, 1995) and therefore flow rate is strongly modulated, because it is approximately proportional to the width to the power of three. Our study principally explores the effects of dyke geometry taking into account elastic wallrock deformation. For other parameters we have used the magma system properties of the Soufrière Hills volcano as a case study.

We present a parametric study of the dyke-fed lava dome eruptions. We discuss the nature of volcanic conduits in lava dome eruptions and make the case that both dyke and cylindrical geometries can occur and co-exist. We develop a mathematical model for a deeper dyke connected to a shallow cylindrical conduit. We present the results with a comparison to the cylindrical case. We show that elastic deformation of the dyke wall can lead to periodic behaviour with time-scales that are typically shorter than the periods associated with the magma chamber. Moreover more complex multi-periodic patterns during magma extrusion cycle are possible.

This study establishes the main principles and investigates parameter variations within the expected range of conduit geometries in natural systems. Finally we discuss the implications of the model results for interpreting eruptive behaviours, geophysical phenomena and petrological features of lava dome rocks.

1.1. Volcanic conduits for lava dome eruptions

There is an evidence that the conduits that feed lava dome eruptions can be both dykes and approximate as cylinders. Dykes of a few metres width are commonly observed in the interior of eroded andesite volcanoes. Dykes have been intersected at Inyo crater domes (Mastin and Pollard, 1988) and the 1991–1995 Mount Unzen lava dome (Nakada and Eichelberger, 2004) during drilling projects. Geophysical studies also point to dyke feeders; for example fault-plane solutions of shallow volcano-tectonic earthquakes indicate pressure fluctuations in dykes (Roman, 2005; Roman et al., 2006). Deformation data at Unzen combined with structural analysis indicates that the 1991–1995 dome was fed by a dyke (Nakada et al., 1999). Dykes are also the only viable mechanism of developing a pathway through brittle crust from a deep magma chamber to the surface in the initial stages of an eruption (Rubin, 1995).

However, cylindrical conduits can also develop during lava dome eruptions. Commonly early stages of lava dome eruptions involve phreatic and phreatomagmatic explosions that excavate near surface vents and conduits (Yokoyama et al., 1981; Christiansen and Peterson, 1981; Williams and Self, 1983; Swanson and Holcomb, 1999; Sparks and Young, 2002; Ohba and Kitade, 2005). Explosion vents are attributed to interaction of magma rising along a dyke with ground water. Here the cylindrical conduit is confined to relatively shallow parts of the crust, probably of order hundreds of metres depth and <1 km as indicated by mineralogical studies (Ohba and Kitade, 2005). Examples of such initial crater forming activity include Mount Usu, Mt. St. Helens, and Soufrière Hills, Montserrat (Yokoyama et al., 1981; Christiansen and Peterson, 1981; Sparks and Young, 2002). Many lava dome eruptions are also characterised by Vulcanian, sub-Plinian and even Plinian eruptions. Examples include Unzen, Mount St. Helens, Santiaguito and Soufrière Hills (Williams and Self, 1983; Nakada et al., 1999; Swanson and Holcomb, 1999; Sparks and Young, 2002). Here the fragmentation depth may reach to depths of a few kilometres (Mason et al., 2006) with

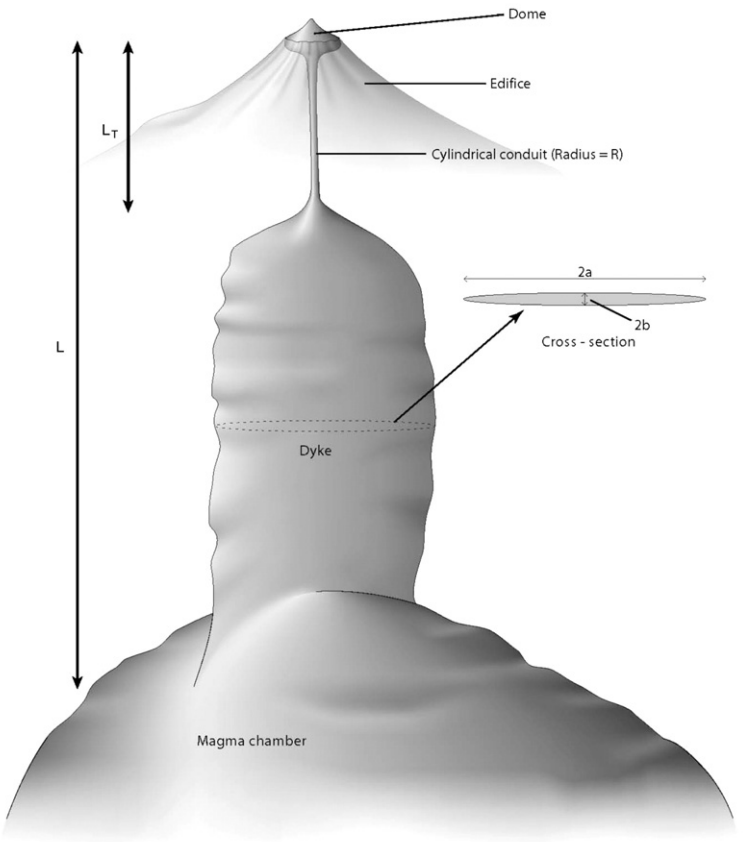

Fig. 1. Schematic view of the volcanic system. In the upper part the conduit is cylindrical with a radius R. A transition from the cylinder to a dyke occurs at depth L_T. The length scale for the transition from cylinder to dyke is w_T. The dyke has an elliptical cross-section with semi-axis lengths a_0 and b_0. The chamber is located a depth L. In the text we used also the following auxiliary variables: $D=2R$ for conduit diameter, $L_d=L-L_T$ for the dyke vertical length, $W_d=2a_0$ for the dyke width, and $H_d=2b_0$ for the dyke thickness.

the possibility of conduit development due to severe underpressuring and mechanical erosion. Subsequently domes can be preferentially fed along the cylindrical conduits created by explosive activity.

This brief summary of conduit development during lava dome eruptions indicates that both dykes and cylindrical conduits can occur. Both can be present together and furthermore can be interconnected to one another. Explosive activity favours cylindrical geometries in the relatively shallow part of the system. In this study for the sake of modelling practicalities we simplify complicated natural geometries by envisaging a deeper dyke of length $L_d=L-L_T$, width $W_d=2a$ and thickness $H_d=2b$ connected to a straight-sided cylinder of length L_T and radius R (see Fig. 1).

2. Governing equations

Melnik and Sparks (2005) modelled the ascent of magma along the conduit from the chamber using a set of 1-D transport equations. In order to generalise the equations to a variable cross-section shape, we assume that the conduit has an elliptical cross-section with area $S=\pi ab$, with a and b major and minor semi-axes, respectively (similar assumptions are made in Mériaux and Jaupart, 1995). We also assume that vertical variations in cross-section area of the dyke occur at length-scales that are much larger than the dyke width; therefore cross-section averaged variables can be used to describe magma flow in the conduit. The set of cross-section averaged equations is now presented.

$$\frac{1}{S}\frac{\partial}{\partial t}(S\rho_m)+\frac{1}{S}\frac{\partial}{\partial x}(S\rho_m V)=-G_{mc}-G_{ph} \quad (1)$$

$$\frac{1}{S}\frac{\partial}{\partial t}(S\rho_{mc})+\frac{1}{S}\frac{\partial}{\partial x}(S\rho_{mc} V)=G_{mc} \quad (2a)$$

$$\frac{1}{S}\frac{\partial}{\partial t}(S\rho_{ph})+\frac{1}{S}\frac{\partial}{\partial x}(S\rho_{ph} V)=G_{ph} \quad (2b)$$

$$\frac{1}{S}\frac{\partial}{\partial t}(S\rho_{\mathrm{d}}) + \frac{1}{S}\frac{\partial}{\partial x}(S\rho_{\mathrm{d}}V) = -J \tag{3a}$$

$$\frac{1}{S}\frac{\partial}{\partial t}(S\rho_{\mathrm{g}}) + \frac{1}{S}\frac{\partial}{\partial x}(S\rho_{\mathrm{g}}V_{\mathrm{g}}) = J \tag{3b}$$

Here t denotes time, x the vertical coordinate, ρ_{m}, ρ_{ph}, ρ_{mc}, ρ_{d} and ρ_{g} are the densities of melt, phenocrysts, microlites, dissolved gas and exsolved gas respectively, and V and V_{g} are the cross-section averaged velocities of magma and gas, respectively. G_{ph}, G_{mc} represent the mass transfer rate due to crystallization of phenocrysts and microlites, respectively, and J the mass transfer rate due to gas exsolution. Eq. (1) represents the mass conservation for the melt phase, Eqs. (2a) and (2b) are the conservation equations for microlites and phenocrysts respectively, Eqs. (3a) and (3b) represent the conservation of the dissolved gas and of the exsolved gas respectively.

$$\frac{\partial p}{\partial x} = -\rho g - 4\mu\frac{a^2+b^2}{a^2b^2}V \tag{4}$$

$$V_{\mathrm{g}} - V = -\frac{k}{\mu_{\mathrm{g}}}\frac{\partial p}{\partial x} \tag{5}$$

Here p is the pressure, ρ the bulk density of magma, g the gravity acceleration, μ is the magma viscosity, k is the magma permeability and μ_{g} is the gas viscosity. Eq. (4) represents the momentum equation for the mixture as a whole in which the pressure drops due to gravity and conduit resistance calculated for laminar flow in an elliptic pipe (see Appendix A). Eq. (5) is the Darcy law for the exsolved gas flux through the magma.

$$\frac{1}{S}\frac{\partial}{\partial t}(S\rho C_{\mathrm{m}}T) + \frac{1}{S}\frac{\partial}{\partial x}(S\rho C_{\mathrm{m}}VT) = L_*(G_{\mathrm{mc}} + G_{\mathrm{ph}}) - TJ - Q_{\mathrm{cl}} + Q_{\mathrm{vh}} \tag{6}$$

Here C_{m} is the bulk specific heat of magma, T is the bulk flow-averaged temperature, L_* is latent heat of crystallization, Q_{cl} denotes the total heat loss by conduction to the conduit walls, and Q_{vh} denotes the total heat generation due to viscous dissipation. Since this paper investigates the effects of conduit geometry and wallrock elasticity on the dynamics, we restrict our study to the case already studied in Melnik and Sparks (2005) where only the latent heat release is considered. This assumption is valid when both $Q_{\mathrm{cl}} \approx 0$ and $Q_{\mathrm{vh}} \approx 0$ or when $Q_{\mathrm{cl}} + Q_{\mathrm{vh}} \approx 0$. Studies of the effects of heat loss and viscous heating require intrinsically two-dimensional approach (Costa and Macedonio, 2003, 2005). Cross-sectional variations in viscosity due to changes in temperature, crystal content and gas exsolution will lead to deviations of a parabolic velocity profile. This in turn will change overall conduit resistance and the relationship between discharge rate and driving pressure. Because the system is strongly non-linear, this deviation may be large. The study of these effects and their parameterization is the subject of ongoing research.

$$\rho_{\mathrm{m}} = \rho_{\mathrm{m}}^0(1-\alpha)(1-\beta)(1-c);\ \rho_{\mathrm{c}} = \rho_{\mathrm{c}}^0(1-\alpha)\beta \tag{7a}$$

$$\rho_{\mathrm{d}} = \rho_{\mathrm{m}}^0(1-\alpha)(1-\beta)c;\ \rho_{\mathrm{g}} = \rho_{\mathrm{g}}^0\alpha \tag{7b}$$

$$\rho = \rho_{\mathrm{m}} + \rho_{\mathrm{c}} + \rho_{\mathrm{d}} + \rho_{\mathrm{g}} \tag{7c}$$

$$\alpha = \frac{4}{3}\pi r_{\mathrm{b}}^3 n;\ \ \frac{\partial}{\partial t}(Sn) + \frac{\partial}{\partial x}(SnV) = 0;\ \ p = \rho_{\mathrm{g}}^0 RT. \tag{8}$$

Here α is the volume concentration of bubble, β the volume concentration of crystals, and c is mass concentration of dissolved gas, ρ_0^{m} denotes the mean density of the pure melt phase, ρ_0^{c} is density of the pure crystal phase (with $\rho_{\mathrm{c}} = \rho_{\mathrm{ph}} + \rho_{\mathrm{mc}}$, $\beta = \beta_{\mathrm{ph}} + \beta_{\mathrm{mc}}$), r_{b} is the bubble radius, and n the number density of bubble per unit volume. Concerning the parameterization of mass transfer rate functions, we use:

$$J = 4\pi r_{\mathrm{b}} n D\rho_{\mathrm{m}}^0\left(c - C_{\mathrm{f}}\sqrt{p}\right) \tag{9}$$

$$G_{\mathrm{mc}} = 4\pi\gamma_{\mathrm{mc}}\rho_{\mathrm{c}}^0(1-\beta)(1-\alpha)U(t)\int_0^t I(\omega)\left(\int_\omega^t U(\eta)\mathrm{d}\eta\right)^2\mathrm{d}\omega \tag{10a}$$

$$G_{\mathrm{ph}} = 3\gamma_{\mathrm{ph}}\left(\frac{4\pi N_{\mathrm{ph}}\beta_{\mathrm{ph}}^2}{3}\right)^{1/3}\rho_{\mathrm{c}}^0(1-\beta)(1-\alpha)U(t). \tag{10b}$$

Here J is parameterized using the analytical solution based on the square-root solubility law suggested for silicate melts (Navon and Lyakhovsky, 1998), U is the linear crystal growth rate ($\mathrm{m\,s^{-1}}$), I is the nucleation rate ($\mathrm{m^{-3}\,s^{-1}}$), which defines the number of newly nucleated crystal per cubic metre, and γ_{mc} and γ_{ph} are two shape factors of the order of unity. Concerning the mass transfer due to crystallization G_{mc} we adapt a model similar to that described in Hort (1998). Assuming spherical crystals, the Avrami–Johnson–Mehl–Kolmogorov equation

in the form adopted by Kirkpatrick (1976), for the crystal volume increase rate, is:

$$\frac{\mathrm{d}\beta}{\mathrm{d}t} = 4\pi Y_t U(t) \int_0^t I(\omega) \left(\int_\omega^t U(\eta)\mathrm{d}\eta \right)^2 \mathrm{d}\omega$$

where $Y_t=(1-\beta)(1-\alpha)$ is the volume fraction of melt remaining uncrystallized at the time t. Therefore, we have $G_{\mathrm{mc}}=\rho_{\mathrm{mc}}\mathrm{d}\beta/\mathrm{d}t$. For the phenocryst growth rate G_{ph} we assume that it is proportional to the phenocryst volume increase rate $\mathrm{d}\beta_{\mathrm{ph}}/\mathrm{d}t=4\pi R_{\mathrm{ph}}^2 N_{\mathrm{ph}} U(t)$ times the crystal density ρ_{c}^0 times the volume fraction of melt remaining uncrystallized at the time t, i.e. $Y_t=(1-\beta)(1-\alpha)$. A detailed description of the parameterization used for the different terms is reported in Melnik and Sparks (2005).

For parameterizations of magma permeability k and magma viscosity μ we use:

$$k = k(\alpha) = k_0 \alpha^j \tag{11}$$

$$\mu = \mu_{\mathrm{m}}(c,T)\theta(\beta)\eta(\alpha,Ca) \tag{12}$$

where k is assumed to depend only on bubble volume fraction α (e.g., Costa, 2006) and here is empirically described as a power of α. Magma viscosity μ depends on water content, temperature, crystal content, bubble fraction and capillary number as described in detail in Section 2.1.

Regarding equations for semi-axes, a and b, we assume that the elliptical shape is maintained and that pressure change gradually in respect with vertical coordinate and time so that the plain strain analytical solution for an ellipse subjected to a constant internal overpressure (Muskhelishvili, 1963; Mériaux and Jaupart, 1995) remains valid:

$$a = a_0 + \frac{\Delta P}{2G}[-(1-2v)a_0 + 2(1-v)b_0] \tag{13a}$$

$$b = b_0 + \frac{\Delta P}{2G}[2(1-v)a_0 - (1-2v)b_0] \tag{13b}$$

where ΔP is the overpressure, i.e. the difference between conduit pressure and far field pressure (here assumed lithostatic for a sake of simplicity), a_0 and b_0 are the initial values of the semi-axes, v is the host rock Poisson ratio, and G is host rock rigidity (shear modulus). The cross section form can range from a circle ($W_{\mathrm{d}}=H_{\mathrm{d}}$) to a flat crack ($H_{\mathrm{d}}\approx 0$). Eqs. (13a) (13b) are based on the assumption that elastic deformation can be locally described in the plain strain approximation (Mériaux and Jaupart, 1995). This implies that relationships (13a) and (13b) can be applied only if the local length scales characterising vertical changes in the conduit geometry and in the fluid pressure are much larger than the transversal dimensions of the conduit, i.e. the diameter conduit $D=2R$ or the dyke width W_{D}. Moreover, local relationships (13a) and (13b) are not valid near the surface where both boundary and topographic effects can be important. However, since in our case, in the upper part we assume that the conduit is a cylinder, deformation effects are not significant in that region.

In order to get a smooth transition from the dyke at depth to a cylindrical conduit the value of a_0 is parameterized as:

$$a_0(x) = A_1 \arctan\left(\frac{x - L_{\mathrm{T}}}{w_{\mathrm{T}}}\right) + A_2 \tag{14}$$

Here L_{T} and w_{T} are the height and the vertical extent of the cylinder to ellipse transition zone and constants A_1 and A_2 are calculated to satisfy conditions $a_0(L)=R$ and $a_0(0)=a_0$, where R is the radius of the cylindrical part of the conduit and a_0 is the length of major dyke semi-axis at the inlet of the dyke. The value of b_0 is calculated in order to conserve the cross-section area of the unpressurized dyke, although it can also be specified independently. The transition represented by Eq. (14) for the parameters listed in Table 1 ($w_{\mathrm{T}}=100$ m) implies a fairly abrupt transition from a dyke to a cylinder. This is justified based on the inference that explosions will excavate a conduit to a well-defined depth and is supported by observations to eroded conduit, such as kimberlites and alkali basalts, where exposures of transitions between feeding dykes and the base of volcanic pipes can be observed (Delaney and Pollard, 1981; Delaney and Gartner, 1997; Sparks et al., 2006).

A sketch of the considered geometry is shown in Fig. 1. Notations and values of the parameters used in the simulations are reported in Table 1.

2.1. Rheological model

Magma viscosity is modelled as a product of melt viscosity $\mu_{\mathrm{m}}(c, T)$, the relative viscosity due to crystal content $\theta(\beta)=\Theta(\beta)\varphi(\beta)$, and the relative viscosity due to the presence of bubbles $\eta(\alpha, Ca)$. Viscosity of the pure melt $\mu_{\mathrm{m}}(c, T)$ is calculated according to Hess and Dingwell (1996). Viscosity increase due to the presence of the crystals is described through the function $\Theta(\beta)$ (Costa, 2005). As crystallization proceeds the remaining melt becomes more silica rich and viscosity increases. The parameterization of this effect (Dirksen et al., 2006) is described through the function $\varphi(\beta)$.

Table 1
Parameters used in the simulations

Notation	Description	Value
C_0	Concentration of dissolved gas	6 wt.%
C_f	Solubility coefficient	4.1×10^{-6} Pa$^{-1/2}$
C_m	Specific heat	1.2×10^{3} J kg^{-1} K^{-1}
R	Conduit radius	15 m
I_0	Max nucleation rate	3×10^{10} m^{-3} s^{-1}
K_0	Permeability coefficients	5×10^{-12} m^2
j	Porosity exponent	3.5
G	Rigidity of host rocks (range)	1.5–6/6–24 GPa
L	Reference length of the conduit	5 km
L_*	Latent heat of crystallization	3.5×10^{5} J kg^{-1}
Q_{in}	Magma chamber influx (range)	2–5 m^3/s^{-1}
R_g	Gas constant	460 J kg^{-1} K^{-1}
R_{ph}	Phenocryst size	5 mm
T_{ch}	Temperature in the magma chamber	860 °C
U_0	Max growth rate	2×10^{-9} m/s^{-1}
V_{ch}	Magma chamber volume (range)	5–50 km^3
β_{ch*}	Chamber crystal content	0.5
ΔT_i	Max undercooling for nucleation	90 K
ΔT_u	Max undercooling for growth	60 K
γ_{mc}	Microlites shape factor	0.238
γ_{ph}	Phenocrists shape factor	0.460
ν	Poison ratio of host rocks	0.3
μ_g	Gas viscosity	1.5×10^{-5} Pa s
ρ_c	Density of crystals	2700 kg m^{-3}
ρ_m	Density of the melt	2300 kg m^{-3}
ρ_r	Density of wallrocks	2600 kg m^{-3}
Rheological model parameters		
β_*; γ; δ	Viscosity change with crystal fraction	0.67; 3.99; 16.94
$\theta(\beta_*)$	Implicit value for ε	3288
a_1; a_2	Viscosity change with melt composition	4.33; 10.48
Conduit geometry parameters		
L	Magma chamber depth (range)	4–8 km
L_T	Transition depth (range)	1–2 km
w_T	Transition width length	100 m
W_d	Width of dyke (range)	30–900 m
H_d	Thickness of dyke (range)	3–30 m

Effects of solid fraction are parameterized as follows (Costa, 2005):

$$\Theta = \frac{1+\left(\frac{\beta}{\beta_*}\right)^{\delta}}{\left(1-\varepsilon\, erf\left\{\frac{\sqrt{\pi}}{2\varepsilon}\frac{\beta}{\beta_*}\left[1+\left(\frac{\beta}{\beta_*}\right)^{\gamma}\right]\right\}\right)^{2.5\beta_*}} \qquad (15a)$$

where β_* represents the critical transition fraction, γ is a measure of the steepness of the rheological transition, ε ($0<\varepsilon<1$) determines the value of $\Theta(\beta_*)$, i.e. $\Theta(\beta_*) = 2\times\left[1-\varepsilon\,\mathrm{erf}\left(\sqrt{\pi/\varepsilon}\right)\right]^{-2.5\beta*}$, and δ controls the increase of Θ as β tends toward one. In principle β_*, γ, δ and ε can be a function of the strain rate and crystal shape but here are assumed to be constant. The correction due to the change in composition is empirically described as in Dirksen et al. (2006):

$$\phi(\beta) = \exp\left[a_1(\beta-\beta_{ch*}) + a_2(\beta-\beta_{ch*})^2\right] \qquad (15b)$$

where a_1 and a_2 are empirical coefficients and β_{ch*} is the initial crystal content.

Relationships (15a) and (15b) produce much stronger dependence of the viscosity on crystal content than those used in Melnik and Sparks (2005). Increase in crystal content from 50 to 80 vol% leads to an increase in viscosity by a factor of 2.15×10^{8} using Eqs. (15a) and (15b) but only by a factor of 3.1×10^{2} in the case of the correction used in Melnik and Sparks (2005). As we will show this difference results in not only quantitative but also qualitative effects.

Effects due to the presence of bubbles are accounted for adopting a generalisation of Llewellin and Manga (2005):

$$\eta(\alpha, Ca) = \frac{1}{1+25Ca^2}\left[\frac{1}{(1-\alpha)} + 25Ca^2(1-\alpha)^{5/3}\right] \qquad (15c)$$

where $Ca=\lambda\dot{\varepsilon}$ is the capillary number, $\lambda=\mu_m r_b/\Gamma$ a characteristic bubble time-scale (Γ is the bubble–liquid interfacial tension with a value of $\approx$0.25 N m^{-1}) and $\dot{\varepsilon}$ is the shear strain-rate averaged on the elliptical cross section calculated as explained in Appendix A.

2.2. Boundary and initial conditions

Eqs. (1) (2a) (2b) (3a) (3b) (4) (5) (6) (7a) (7b) (7c) (8) (9) (10a) (10b) (11) (12) (13a) (13b) are solved by using the numerical method described in Melnik and Sparks (2005) between the top of the magma chamber and the bottom of the lava dome that provides some constant load. The effects of dome height and morphology changes are not considered in this paper. We consider three different kinds of boundary conditions at the inlet of the dyke: constant pressure, constant influx rate and presence of the magma chamber that is located in elastic rocks. The case of constant pressure is applicable when a dyke starts from a large magma unspecified source so that changes in the pressure in the source region remain small. An estimate of a volume of magma stored in the source region that allows pressure to be constant depends on wallrock elasticity, magma compressibility (volatile content) and the total volume of the erupted material. If the magma flow at depth is controlled by regional tectonics the case of constant influx rate into the dyke may be applicable if total

variations in supply rate are relatively small on the timescale of the eruption.

In the case of magma storage prior to the eruption in a shallow magma chamber and significant chamber replenishment, the flow inside the conduit must be coupled with the model for the magma chamber. In this case, as explained in detail in Melnik and Sparks (2005), we assume that the relationship between the pressure at the top of the magma chamber p_{ch} and the intensity of influx Q_{in} and outflux Q_{out} of magma to and from the chamber is given by:

$$\frac{dp_{ch}}{dt} = \frac{4G\langle K\rangle}{\langle\rho\rangle V_{ch}(3\langle K\rangle) + 4G)}(Q_{in} - Q_{out}) \quad (16)$$

where V_{ch} is the magma chamber volume, $\langle\rho\rangle$ and $\langle K\rangle$ the average magma density and magma bulk modulus respectively, and G is the rigidity of rocks surrounding the chamber.

The cases of constant influx and of constant source pressure are the limit cases of Eq. (16) in the case of infinitely small and infinitely large chamber volumes.

We use a steady-state distribution of parameters along the conduit as an initial condition for the transient simulation.

3. Results of numerical simulations

In this section we investigate the influence of controlling parameters on magma flow behaviour. As in previous studies (Melnik and Sparks, 1999; Barmin et al., 1999; Melnik and Sparks, 2005), for all the calculations we use a reference set of parameters (see Table 1) which are typical for Soufrière Hills Volcano, Montserrat. This study concerns geometrical effects of the conduit and wallrock rigidity, therefore, the governing parameters for magma will remain constant throughout the simulations. Melnik and Sparks (2005) explored variations in magma properties and conduit dimensions for the cylindrical case. We have not made such a wide parametric study here because our purpose is to isolate and investigate variations in conduit geometry and elasticity effects.

3.1. Influence of rheology on eruption dynamics

In this paper we adopt a new rheological model (see Eq. (15a) (15b)). We first explore the effects that new rheology introduces on the dynamics for the case of an undeformable cylindrical conduit and compare these results with previous calculations (Melnik and Sparks, 2005) with all other parameters being the same (Table 1). In simulations of Melnik and Sparks (2005), when Q_{in} in Eq. (16) corresponds to the intermediate regime, the period of discharge rate variation was proportional to the chamber size. The upper and the lower branches of the steady-state solution were stable irrespective of the magma chamber size. For very small magma chamber volumes the intermediate solution became stable. The steady state solution, in the case of new rheology, is shifted to much larger pressures (Fig. 2) for two reasons. First the new rheology leads to higher conduit friction and thus larger pressure drops (see Eq. (4)). Second, the weight of the magma that enters the conduit at higher pressures also increases due to lower vesiculation, leading to an increase in the pressure drop due to gravity.

The transient evolution of the eruption in the case of the rheology used in Melnik and Sparks (2005) leads to stabilization of eruption at all values of Q if a fixed influx rate is used as a boundary condition. In the case of the fixed source pressure boundary condition the upper and the lower regimes are stable. If the starting point corresponds to the intermediate regime the solution jumps to the upper regime and stabilizes there.

In the case of the new rheology there is a range of influxes (between 2.5 and 4.7 m^3/s) when the system generates short period (4.5 to 6 days) non-damping oscillations with complicated shapes (Fig. 2). Two local minima exist during one period in the pattern. Outside this

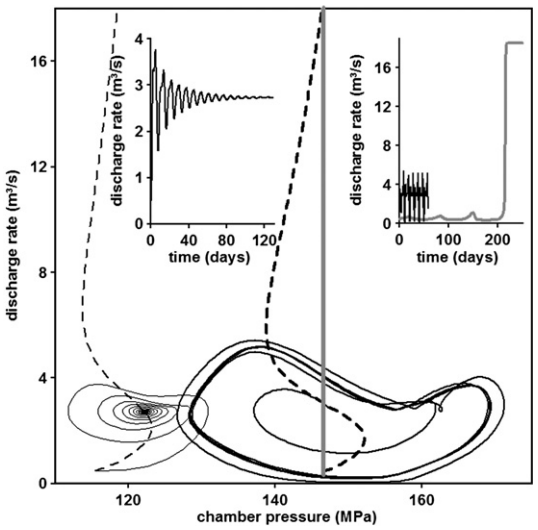

Fig. 2. Effects of different rheologies on the cyclicity of an undeformable cylindrical conduit. Dependence of discharge rate on the pressure at the bottom of the conduit when rheology relationships (15) are used (thick line) with the rheology from Melnik and Sparks (2005) (thin line). Dashed lines show the corresponding steady-state solutions. The thick grey line shows the case when the transient solution is not stable with respect to fixed source pressure boundary condition and a jump to the upper regime of the steady-state solution occurs. The evolution of discharge rates is also shown in the insets.

range of influx the solution stabilizes with time. There is also a range of starting points at the lower branch of the steady-state solution where the transient solution is not stable with respect to fixed source pressure boundary condition. The solution, after a few small scale oscillations with increasing amplitude, jumps to the upper regime of the steady-state solution and stabilizes there (grey line).

The explanation of these different results can be understood in terms of the contrasts between the two rheologies in terms of functional form, sharpness and amplitude of viscosity variation with crystal content. We found that the main cause of the change in stability of the steady state solution is due to the sharpness of viscosity increase with crystal content.

3.2. Rigidity and influence of dyke geometry

Rigidity values are not well constrained in volcanic systems because of the presence of fractures and high temperatures. Both measurements in laboratory (Voight et al., 1999) and best-fits for ground deformation (Beauducel et al., 2000; Voight et al., 2006) and seismicity (Troise et al., 2003) suggest a range of order 1 to 10 GPa. Typically values of rigidity are larger from seismic data than from inversion of deformation data and laboratory results (e.g., Jaeger and Cook, 1976). Here we consider results from deformation studies as more relevant (Voight et al., 2006). As a reference case we assume that rigidity G linearly increases with depth

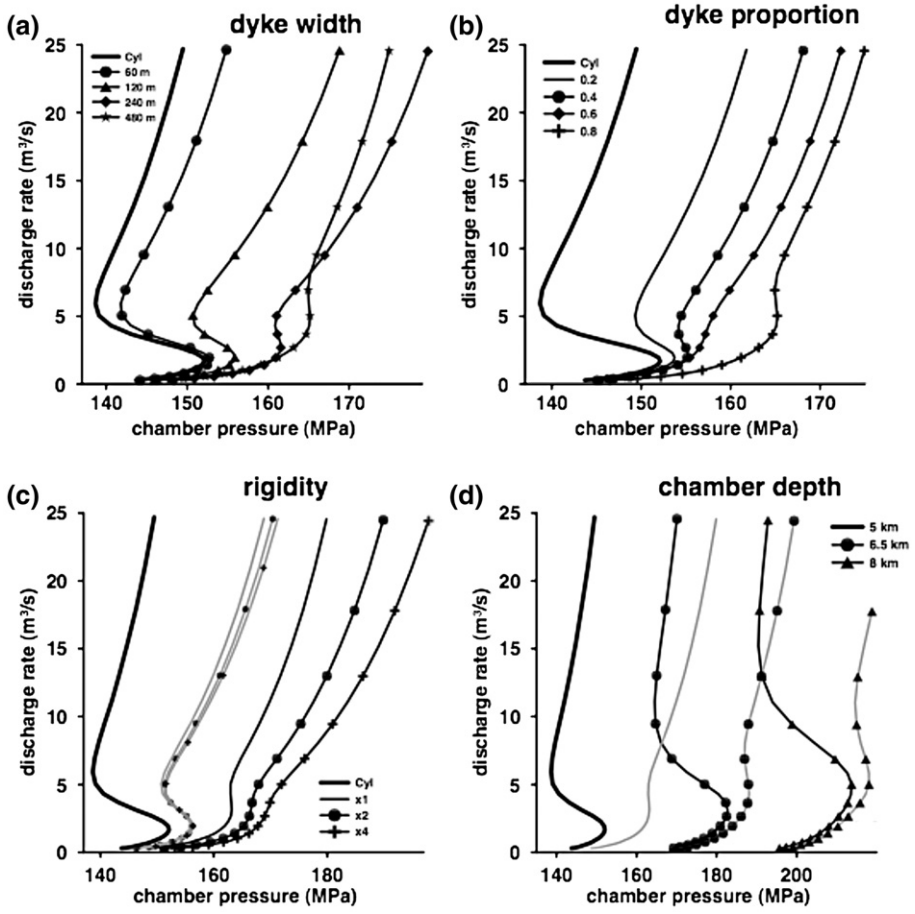

Fig. 3. A set of steady state solutions. Dependence of discharge rate on chamber pressure. (a) Influence of the dyke width W_d (see Fig. 1 for details). The conduit diameter at the top is fixed at 30 m. (b) Influence of the proportion of the conduit occupied by the dyke. Calculations are presented for the dyke width W_d=480 m. As a reference the solution for cylindrical conduit having a diameter D=30 m is shown by a thick solid line. (c) Influence of the depth of the magma chamber. Solid lines correspond to the solutions with cylindrical conduit, dashed — to the dyke width W_d=300 m. The transition from the dyke to cylindrical conduit is fixed at depth of 1 km below the surface. (d) Influence of the wallrock rigidity. A linear profile of the rigidity is assumed. At the Earth surface, the rigidity modulus is equal to 1.5 GPa, at depth of 5 km the rigidity modulus is equal to 6 GPa. The values of rigidity are multiplied by a factor n so that curves for "x4" correspond to the range of rigidity from 6 to 24 GPa. Solid lines correspond to the dyke width W_d=300 m, dashed lines are for the dyke width W_d=120 m. As a reference the solution for cylindrical conduit is shown by a thick solid line.

having a value of 1.5 GPa at the surface and 6 GPa at a depth of 5 km with a Poisson ratio $\nu = 0.3$.

Fig. 3 represents a set of steady-state solutions and controls of the main geometrical parameters including the dyke width, i.e. $W_d = 2a_0$ (Fig. 3a); the proportion of the conduit occupied by a dyke, i.e. L_d/L (Fig. 3b); and the magma chamber depth, i.e. L (Fig. 3c). Fig. 3d shows a set of steady-state solutions for different rock rigidities. For the curves marked as "xn" the values of rigidity at all depths are multiplied by a factor of n. At all plots the reference case of cylindrical conduit is shown with a thick solid line. The vertical extent of the transition zone, w_T, from a dyke to a cylinder to ellipse transition zone w_T was assumed to be 100 m. This value is about three times the conduit diameter, allowing us to extrapolate the analytical solutions (13a) and (13b) in the transition region. This represents a compromise between having a rapid change from dyke to cylinder and verifying the condition $w_T \gg D$ that can be considered fully verified everywhere except for a very narrow region.

The conduit friction for a dyke-shape conduit is larger than for a cylindrical conduit of the same cross-sectional area because the friction is controlled by the perimeter of the dyke that increases as the ratio between larger and smaller semi-axes of the ellipse increases. Therefore, dykes require large chamber pressures in order to sustain the same discharge rate; this point is illustrated in Fig. 3a. At low discharge rates when the influence of friction is relatively small due to low velocity the difference between the solutions for a cylinder and a dyke is small and rapidly increases with the increase in discharge rate. For large widths of the dyke widens strongly with magma overpressure reducing the friction. The shift in steady-state solutions to larger pressure is not monotonic (compare curves for $W_d = 240$ and 480 m in Fig. 3a). As the proportion of the conduit occupied by a dyke decreases (the depth of the transition to cylindrical conduit increases), the steady-state solution tends to that for the cylinder (Fig. 3b). Increase in magma chamber depth leads to a progressive shift of the solutions to higher chamber pressures due to the increase in overall weight of the magma column and conduit resistance (Fig. 3c). Also, the transition points between branches of steady-state solution move to higher discharge rates because magma in a longer conduit has a longer ascent time for the same discharge rate and, thus, more efficient crystal growth (Fig. 3c). As wallrock rigidity increases the dyke ability to expand decreases leading to a shift of the solution to larger chamber pressures. The effect is more pronounced for large dyke widths W_d (Fig. 3d).

Fig. 4 shows the transient evolution of eruption dynamics for three different boundary conditions at the inlet of the dyke. In the case of fixed influx into the dyke, the pressure during the cycle oscillates with large amplitude allowing the dyke to change its volume significantly, providing temporary storage for the magma. The period of pulsations is much longer (around 10 days) than for the case of the cylinder. Thus, the presence of the dyke increases effective compressibility of the system. When a magma chamber is present the system eventually oscillates with nearly constant pressure and thus the shape of discharge rate curve with time is similar to those for a constant source pressure boundary condition; there is a sharp increase in discharge rate following by a more gentle decrease. For the case of fixed influx rate the

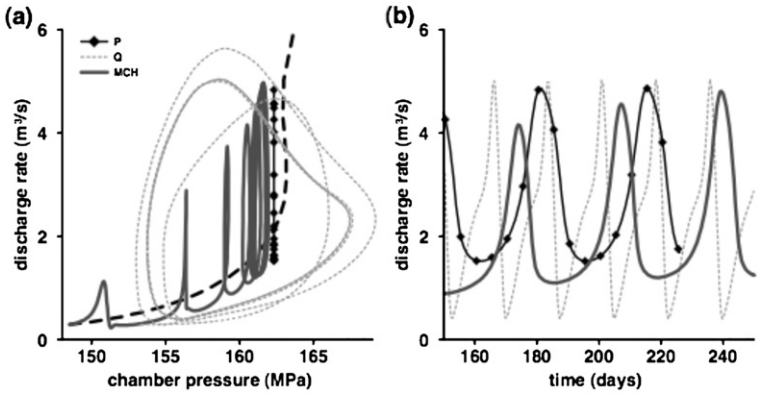

Fig. 4. Influence of the boundary condition at the bottom of the dyke on the evolution of discharge rate. (a) Dependence of discharge rate on the pressure at the bottom of the dyke. (b) Discharge rate evolution at the surface with time. Dashed line on Fig. 4a represents the steady-state solution for a dyke width $W_d = 300$ m. Thick solid grey line corresponds to the case when conduit flow is coupled with the magma chamber of $V_{ch} = 25$ km^3 with an influx rate of $Q_{in} = 2.5$ m^3/s, thin dashed grey line corresponds to the case of constant influx into the bottom of the dyke of 2.5 m^3/s, thick solid black line with diamonds corresponds to a fixed pressure at the bottom of the dyke (in Fig. 4a it is represented by a vertical line).

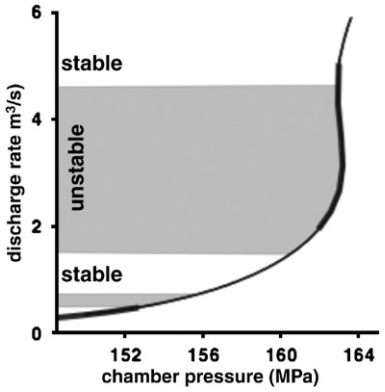

Fig. 5. Stability ranges for the case of different boundary conditions for a dyke width W_d=300 m. Regions of steady state solution marked by a thick black line are unstable in respect with fixed source pressure boundary condition. The shaded grey regions define where the steady-state solution is unstable with respect of fixed influx boundary condition.

shape of the signal is the opposite. After gradual increase in discharge rate there is a rapid decrease. The period of pulsation is less than half of that for the case of fixed source pressure or with a magma chamber.

Fig. 5 shows an example of stability ranges for the case of different boundary conditions. Regions of steady state solution marked by a thick line are unstable in respect with fixed source pressure boundary condition. Shaded grey regions define where the steady-state solution is unstable with respect to fixed influx boundary condition. These regions partly overlap leading to unstable behaviour irrespective of the boundary condition. Because fixed source pressure and fixed influx rate represent the limit cases of the generic boundary condition (16) for the cases of infinitely large and infinitely small volume of the magma chamber, respectively, the stability ranges for large but finite chamber volumes tend to stability ranges for the fixed source pressure. Stability ranges for small chamber volumes tend to stability ranges for the fixed influx. In all cases of boundary conditions the upper regime remains stable. In previous studies (Barmin et al., 1999; Melnik and Sparks, 2005) only the intermediate regime of the steady-state solution was unstable if the magma chamber volume was larger than the critical value.

Fig. 6 presents the dependence of period of pulsations for different boundary conditions (for fixed source pressure, influx rate and different chamber volumes) on the intensity of magma supply to the dyke or magma chamber (Fig. 6a), and the influence of dyke width for a fixed magma chamber volume. In the case of a cylinder the dependence of the period on the intensity of influx into the magma chamber is not monotonic. The period has a minimum in the middle between transition points between the lower, intermediate and upper branches of the steady-state solution and increases significantly when influx rate tends to the lower transition point (see Fig. 7 in Melnik and Sparks, 2005).

In the case of large dyke widths (Fig. 6a), the period monotonically increases with the increase in influx into the chamber. With respect to the magma chamber volume there are two distinct behaviours. At low influx rate the period becomes short and independent on the chamber volume. Its value is totally controlled by the elastic properties of the dyke. We call this the dyke-dominated regime. In the case of high influx rate the period increases with the increase in magma chamber volume. We call this the chamber-dominated regime. The influence of the magma chamber on the period increases with increase in the influx rate. If the constant influx from the source region is applied as a boundary condition the period of pulsations monotonically decreases with increase in the intensity of the influx. In the

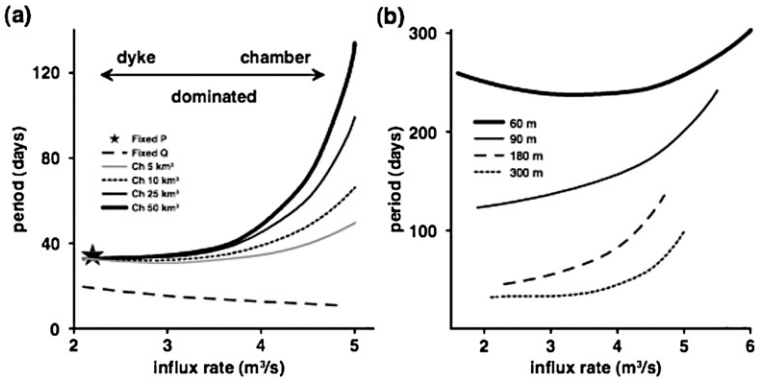

Fig. 6. Dependence of the period of pulsations on the magma influx rate for different chamber volumes for a dyke width W_d=300 m (a); results for a fixed source pressure (star) and fixed inflow rate into the dyke (long dashed line) are also reported for comparison. Fig. 6b shows the influence of dyke width W_d for a magma chamber volume of V_{ch}=25 km^3.

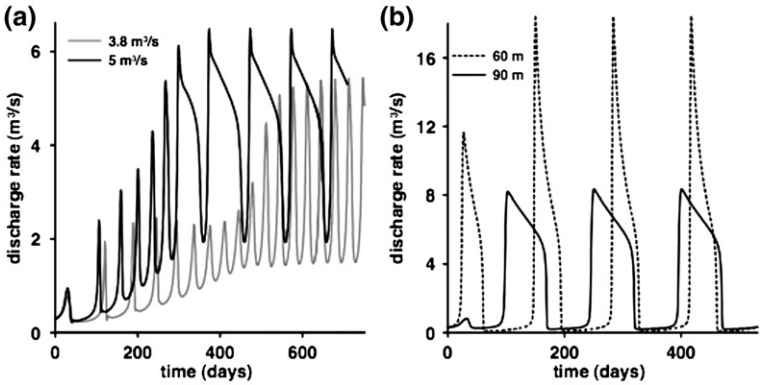

Fig. 7. Dependence of discharge rate on time for the case of coupling with a magma chamber of volume 25 km^3 for (a) a fixed width W_d=300 m and influx rates of Q_{in}=3.8 m^3/s (grey line) and Q_{in}=5 m^3/s (black line), and for (b) a fixed influx rate Q_{in}=3.8 m^3/s and dyke widths of W_d=60 m (dashed line) and W_d=90 m (solid line).

reported example it is 2 to 3 times shorter than for the case of dyke-dominated regime.

Fig. 6b shows that the period decreases with increasing dyke width. As the dyke width decreases and the dyke becomes more cylindrical, the period increases tend to the values similar to cylinders. The dependence of period on the influx rate also becomes non-monotonic as for the case of cylindrical conduit.

Fig. 7a gives an explanation for the presence of dyke- and chamber-dominated regime. The eruption starts with low discharge rate and for both intensities of influx rate initially the period of pulsations is small and dyke dominated. With time for the case of the high influx rate the average discharge rate during one period of oscillations increases. The dyke cannot respond to rapid changes in discharge rate and the chamber influence becomes dominant. The shape of pulsation also changes from more symmetrical to pulsations with a sharp increase in discharge rate and then gradual decrease. For the comparison calculations with shorter dyke width are shown in Fig. 7b. The shape of the cycle is strongly asymmetrical. Due to the shape of the steady-state solution (see Fig. 3a), discharge rate during the cycle reaches very low values and the eruption nearly stops.

Fig. 8 shows the evolution of discharge rate with time for the different influx intensities for the magma chamber depth of 6.5 km (Fig. 8a) and dependence of the period of pulsations on the intensity of influx rate for different chamber depths (Fig. 8b). A striking new feature in comparison with smaller chamber depth is the presence of multiple period solutions (compare Fig. 8a for Q_{in}=4.5 m^3/s and Fig. 7a). There are two distinct periods of pulsations present. Low amplitude oscillations occur with a period typical for the dyke-dominated regime, whereas large spikes in discharge rate occur with the period that is controlled by the magma chamber size. The branches of the solutions that have multiple period oscillations are marked by a thick line in Fig. 8b.

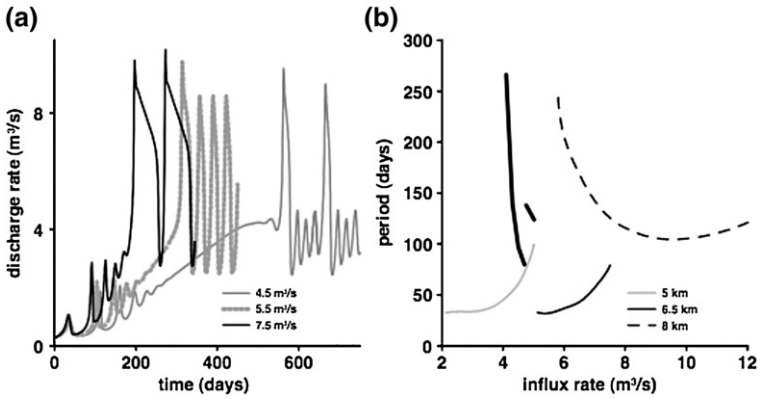

Fig. 8. Dependence of discharge rate on time for the case of coupling with a magma chamber of volume 25 km^3 located at a depth of 6.5 km for a dyke with W_d=300 m and different influx rates (a). Dependence of period of pulsation on influx rate for different depths (as reported) of a magma chamber of volume V_{ch}=25 km^3 and a fixed width W_d=300 m (b). Solutions with multiple periods are marked with a thick line.

The number of short period pulses in between the large pulses can vary with influx rate. This is why the small variation in influx rate leads to large variations in the period of pulsation (which is calculated as a time difference between two large pulses). If the volume of the magma chamber increases the number of short period pulses increases, but the amplitude of these pulses decreases. The overall period increases nearly linearly with magma chamber volume. For small magma chamber volumes the solution tends to a regime with only one period that is controlled by the dyke. For the larger chamber depth (8 km) influx rates that correspond to pulsatory regime are much larger and the system is always in chamber dominated regime. The period of pulsations is much longer than for the case of shallow magma chamber.

The increase in the transition depth between the dyke and the cylindrical part of the conduit (shortening of the dyke part) leads for the solution that is closer in behaviour to a cylindrical conduit. The period of pulsations increases in dyke dominated regime by 25% and for the chamber dominated regime only by 9% when the dyke proportion decreases from 0.8 to 0.4.

The effect of rigidity on the period of pulsation was found to be rather weak. Increase in rigidity by a factor of 4 decreases the period of pulsations in dyke dominated regime by less than 20%. In the chamber dominated regime, the influence of rigidity is even weaker because in the magma chamber the bubble concentration is sufficiently large so that the influence of magma compressibility on the pressure is stronger than the influence of the rigidity.

4. Discussion and conclusion

Introduction of dyke geometry together with elastic wallrock deformation and more complex conduit architecture with interconnected dykes and cylindrical parts further complicates the possible behaviours of lava dome eruptions. Our study shows that the behaviour depends on the boundary conditions and that there can be two time-scales of periodicity, one associated with the magma chamber and the other associated with the conduit system. This time-scale is typically shorter than the time-scale related to the magma chamber. Some of the models are dominated by one or the other of these time-scales, but some show both. Period of pulsation can also evolve with time.

With respect to the results of Melnik and Sparks (2005), two new mechanisms can cause cyclicity on different time-scales. The first mechanism, with a period from few days to a week, is associated with rheology and compressibility of magma. The second mechanism, with a period from few to several weeks, is due to the elasticity of the conduit walls. In presence of a sharp rheological transition at critical crystal content, the formation of a plug in the upper part of the conduit can occur. A relatively bubbly rich region can form in the lower part of the conduit increasing magma compressibility and allowing pressure accumulation. When the conduit walls can be elastically deformed, the system is able to store temporarily and locally larger amounts of magma. That will result in larger effective compressibility of the system and, thus, in longer periods of discharge rate pulsations. The conduit acts as a small elastic magma chamber and can generate a cyclic behaviour even when a fixed flux is assumed as boundary condition at the conduit inlet.

We recognise that these models, notwithstanding their complexity, remain far from a complete description of natural systems. Important processes are not yet incorporated into these models; for example viscous dissipation, fully 2-D and 3-D effects, and heat loss to wallrocks. Many parameters are poorly constrained. In particular the conduit architecture is very difficult to characterise in volcanic systems, but is perhaps the most important parameter of all due to the strong sensitivity of magma pressure and discharge rate as illustrated in this study. It is going to be very difficult, perhaps an impossible task, to constrain magma system properties so well in real systems that the models can be used in a fully quantitative way, especially when the system is such that the strong non-linearities make behaviour extremely sensitive to very small changes in parameters. The models can thus be applied to natural systems only in a qualitative way.

Lava dome eruptions are episodic on a variety of time-scales. The Soufrière Hills volcano, Montserrat provides the clearest example with three time-scales. The shortest time-scale of a few hours to a few days is attributed to shallow conduit degassing processes with stick-slip motion of a consolidated plug (Denlinger and Hoblitt, 1999; Dirksen et al., 2006). There is an intermediate scale of order several weeks (Sparks and Young, 2002) that develops intermittently, as well as periods of steady extrusion with no discernible pulsations (Sparks et al., 1998; Wadge et al., 2006). The longest time-scale relates to three periods of extrusion 2 to 3 years alternating with intervening repose durations of 18 months and 2 years, although the number of alternations is too few to claim any periodic behaviour. By introducing a dyke we have shown that two time-scales can be manifested, one associated with the magma chamber and the other with the dyke. The models inevitably become more

complex and all the styles of behaviour observed at SHV and other volcanoes can be reproduced (in a qualitative sense) by simulations. These include: cyclic behaviour dominated by the shorter dyke time-scale; cyclic behaviour dominated by the magma chamber time-scale; periods of steady extrusion with no dominant cyclicity; alternation and superposition of the time-scales of cyclicity; and abrupt transitions between styles of activity. As pointed out by Melnik and Sparks (2005) the models can show extreme sensitivity to very minor changes in system parameters. Complex time series of discharge rate can develop that mimic the observed behaviour.

The models can be applied to the features of the well-documented 5–7 week cycles at SHV (Voight et al., 1999; Sparks and Young, 2002) which show sharp onsets followed by gradual decline in activity. Our study of boundary conditions suggests that this behaviour is more consistent with near constant pressure from a large magma chamber rather than a constant supply rate into the dyke.

Introduction of a dyke into the models also has implications for petrology. The calculated pressure fluctuations can be of order a few tens of MPa. In a water-saturated andesite magma such pressure fluctuations are sufficient to cause quite large changes in mineral equilibria as water goes in and out of solution in response to pressure changes. For example when pressure is increasing water will be dissolved and plagioclase feldspar will be resorbed, while when pressure is decreasing plagioclase feldspar will crystallize due to water exsolution to produce a normal zone. Dissolution surfaces and thin normally zones are common in plagioclase feldspars from andesites (Blundy et al., 2006) with abrupt increases in An content across the discontinuity. Humphreys et al. (2006) have, for example, documented such zoning in the 2001–2003 andesite lava of Shiveluch volcano, Kamchatka and attributed it to the pulsatory behaviour of the volcano.

Our study emphasizes the strong non-linearities and complex behaviours of lava dome eruptions. It seems likely that when 2-D and 3-D effects and other processes, such as viscous heating and heat loss to conduit walls are taken into account, system behaviour may develop chaotic characteristics. From a forecasting and hazard perspective there will be large intrinsic uncertainties in governing parameters that will make volcanic systems in some circumstances principally unpredictable. On the other hand lava dome systems may also develop episodic and systematic behaviours for long periods so that behaviour becomes predictable for a while.

Acknowledgments

This work was supported by NERC research grant reference NE/C509958/1, the Russian Foundation for Basic Research (05-01-00228) and President of Russian Federation program (NCH-4710.2006.1). RSJS acknowledges a Royal Society Wolfson Merit Award. We wish to thank A. Barmin for useful discussions, S. Powell who helped us in drawing the sketch in Fig. 1. We also are grateful to reviewers of the paper, V. Lyakhovskii and anonymous for useful comments that improved the paper.

Appendix A. Calculation of the average shear strain rate for a viscous flow in an elliptical conduit

The velocity profile in a conduit with an elliptical cross-section is (Landau and Lifschitz, 1994):

$$v = \frac{\mu}{2}\frac{\mathrm{d}p}{\mathrm{d}x}\frac{a^2b^2}{a^2+b^2}\left(1-\frac{y^2}{a^2}-\frac{z^2}{b^2}\right) = 2V\left(1-\frac{y^2}{a^2}-\frac{z^2}{b^2}\right) \tag{A1}$$

where V is the average velocity:

$$V = \frac{1}{4\mu}\frac{\mathrm{d}p}{\mathrm{d}x}\frac{a^2b^2}{a^2+b^2} \tag{A2}$$

The shear strain-rate has two components $\partial v/\partial y$ and $\partial v/\partial z$:

$$\frac{\partial v}{\partial y} = -4V\frac{y}{a^2}$$

$$\frac{\partial v}{\partial z} = -4V\frac{z}{b^2} \tag{A3}$$

The square shear strain-rate modulus $\dot{\gamma}^2$ can be expressed in terms of the components (A3) as:

$$\dot{\gamma}^2 = \frac{\partial v^2}{\partial y}+\frac{\partial v^2}{\partial z} \tag{A4}$$

Integrating across the ellipse and dividing by cross-sectional area we obtain the average square shear strain-rate:

$$\langle\dot{\gamma}^2\rangle = \frac{4(a^2+b^2)}{a^2b^2}V^2 \tag{A5}$$

where the brackets denote the average. Defining an average shear strain-rate $\dot{\varepsilon}$ as the square root of Eq. (A5) we have finally:

$$\dot{\varepsilon} \equiv \sqrt{\langle\dot{\gamma}^2\rangle} = 2V\sqrt{\frac{a^2+b^2}{a^2b^2}} \tag{A6}$$

that for $a=b=R$ reduces to the value valid for a cylindrical conduit $\dot{\varepsilon} = 2\sqrt{2}V/R$. If instead to define $\dot{\varepsilon} = \sqrt{\langle\dot{\gamma}^2\rangle}$ we use $\dot{\varepsilon} = \langle\sqrt{\dot{\gamma}^2}\rangle$ as in Llewellin and Manga (2005) for the cylinder case we obtain $\dot{\varepsilon}=8V/3R$ instead of $\dot{\varepsilon} = 2\sqrt{2}V/R$, with a coefficient that is only about 5% different.

References

Barmin, A., Melnik, O., Sparks, R.S.J., 1999. Periodic behavior in lava dome eruptions. Earth Planet. Sci. Lett. 199, 173–184.

Beauducel, F., Cornet, F.H., Suhanto, E., Duquesnoy, T., Kasser, M., 2000. Constraints on magma flux from displacements data at Merapi volcano, Java, Indonesia. J. Geophys. Res. 105 (B4), 8193–8203.

Blundy, J.D., Cashman, K.V., Humphreys, M.C.S., 2006. Magma heating by decompression-driven crystallisation beneath andesite volcanoes. Nature 443, 76–80. doi:10.1038/nature05100.

Cashman, K.V., 1992. Groundmass crystallization of Mount St. Helens dacite, 1980–1986: a tool for interpreting shallow magmatic processes. Contrib. Mineral. Petrol. 109, 431–449.

Cashman, K.V., 2004. Volatile controls on magma ascent and degassing. The State of the Planet: Frontiers and Challenges in Geophysics American Geophysical Union Monograph, 150, pp. 109–124.

Christiansen, R.L., Peterson, D.W., 1981. Chronology of the 1980 eruptive activity. In: Lipman, P.W., Mullineaux, D.R. (Eds.), The 1980 Eruptions of Mount St. Helens, vol. 1250. S. Geological Survey Professional Paper, Washington (844 pp.).

Costa, A., 2005. Viscosity of high crystal content melts: dependence on solid fraction. Geophys. Res. Lett. 32, L22308. doi:10.1029/2005GL02430 (further comments available at http://arxiv.org/abs/physics/0512173).

Costa, A., 2006. Permeability–porosity relationship: a re-examination of the Kozeny–Carman equation based on fractal pore-space geometry. Geophys. Res. Lett. 33, L02318. doi:10.1029/2005GL025134.

Costa, A., Macedonio, G., 2003. Viscous heating in fluids with temperature-dependent viscosity: implications for magma flows. Nonlinear Process. Geophys. 10, 545–555.

Costa, A., Macedonio, G., 2005. Viscous heating effects in fluids with temperature-dependent viscosity: triggering of secondary flows. J. Fluid Mech. 540, 21–38.

Delaney, P.T., Gartner, A.E., 1997. Physical processes of shallow mafic dike emplacement near the San Rafael Swell, Utah. Geol. Soc. Am. Bull. 109, 1177–1192.

Delaney, P.T., Pollard, D.D., 1981. Deformation of host rocks and flow of magma during growth of minette dikes and breccia-bearing intrusions near Ship Rock, New Mexico. Geol. U.S. Geological Survey Professional Paper, vol. 1202 (60 pp.).

Denlinger, R., Hoblitt, R.P., 1999. Cyclic eruptive behavior of silicic volcanoes. Geology 27, 459–462.

Dirksen, O., Humphreys, M.C.S., Pletchov, P., Melnik, O., Demyanchuk, Y., Sparks, R.S.J., Mahony, S., 2006. The 2001–2004 dome-forming eruption of Shiveluch Volcano, Kamchatka: observation, petrological investigation and numerical modelling. J. Volcanol. Geotherm. Res. 155, 201–226. doi:10.1016/j.jvolgeores.2006.03.029.

Green, D.N., Neuberg, J., 2006. Waveform classification of volcanic low-frequency earthquake swarms and its implication at Soufrière Hills Volcano, Montserrat. J. Volcanol. Geotherm. Res. 153 (1–2), 51–63. doi:10.1016/j.jvolgeores.2005.08.003.

Hess, K.U., Dingwell, D.B., 1996. Viscosities of hydrous leucogranite melts: a non-Arrhenian model. Am. Mineral. 81, 1297–1300.

Hort, M., 1998. Abrupt change in magma liquidus temperature because of volatile loss or magma mixing: effects of nucleation, crystal growth and thermal history of the magma. J. Petrol. 39, 1063–1076.

Humphreys, M.C.S., Blundy, J.D., Sparks, R.S.J., 2006. Magma evolution and open-system processes at Shiveluch Volcano: insights from phenocryst zoning. J. Petrol. 47, 2303–2334. doi:10.1093/petrology/egl045.

Jaeger, J.C., Cook, N.G.W., 1976. Fundamental of Rock Mechanics, 2 ed. Chapman and Hall Ltd, London.

Kirkpatrick, R., 1976. Towards a kinetic model for the crystallization of magma bodies. J. Geophys. Res. 81, 2565–2571.

Landau, L., Lifschitz, E., 1994. Physique Theorique — Mecanique des Fluides, 3 ed. MIR, Moscow.

Lister, J.R., Kerr, R.C., 1991. Fluid mechanical models of crack propagation and their application to magma transport in dykes. J. Geophys. Res. 96, 10049–10077.

Llewellin, E.W., Manga, M., 2005. Bubble suspension rheology and implications for conduit flow. J. Volcanol. Geotherm. Res. 143, 205–217.

Mason, R.M., Starostin, A.B., Melnik, O., Sparks, R.S.J., 2006. From Vulcanian explosions to sustained explosive eruptions: the role of diffusive mass transfer in conduit flow dynamics. J. Volcanol. Geotherm. Res. 153, 148–165. doi:10.1016/j.jvolgeores.2005.08.011.

Massol, H., Jaupart, C., Pepper, D.W., 2001. Ascent and decompression of viscous vesicular magma in a volcanic conduit. J. Geophys. Res. 106 (B8), 16223–16240. doi:10.1029/2001JB000385.

Mastin, G.L., Pollard, D.D., 1988. Surface deformation and shallow dike intrusion processes at Inyo Craters, Long Valley, California. J. Geophys. Res. 93 (B11), 13221–13235.

Melnik, O., Sparks, R.S.J., 1999. Nonlinear dynamics of lava dome extrusion. Nature 402, 37–41.

Melnik, O., Sparks, R.S.J., 2005. Controls on conduit magma flow dynamics during lava dome building eruptions. J. Geophys. Res. 110 (B022). doi:10.1029/2004JB003183.

Mériaux, C., Jaupart, C., 1995. Simple fluid dynamic models of volcanic rift zones. Earth Planet. Sci. Lett. 136, 223–240.

Muskhelishvili, N., 1963. Some Basic Problems in the Mathematical Theory of Elasticity. Noordhof, Leiden, The Netherlands.

Nakada, S., Eichelberger, J.C., 2004. Looking into a volcano: drilling Unzen. Geotimes 49 (3), 14–17.

Nakada, S., Shimizu, H., Ohta, K., 1999. Overview of the 1990–1995 eruption at Unzen Volcano. J. Volcanol. Geotherm. Res. 89, 1–22.

Navon, O., Lyakhovsky, V., 1998. Vesiculation processes in silicic magmas. In: Gilbert, J., Sparks, R.S.J. (Eds.), The Physics of Explosive Volcanic Eruption. Special Publication, vol. 145. Geological Society, London, pp. 27–50.

Ohba, T., Kitade, Y., 2005. Subvolcanic hydrothermal systems: implications from hydrothermal minerals in hydrovolcanic ash. J. Volcanol. Geotherm. Res. 145, 249–262. doi:10.1016/j.jvolgeores.2005.02.002.

Roman, D.C., 2005. Numerical models of volcanotectonic earthquake triggering on non-ideally oriented faults. Geophys. Res. Lett. 32. doi:10.1029/2004GL021549.

Roman, D.C., Neuberg, J., Luckett, R.R., 2006. Assessing the likelihood of volcanic eruption through analysis of volcanotectonic earthquake fault-plane solutions. Earth Planet. Sci. Lett. 248, 244–252. doi:10.1016/j.epsl.2006.05.029.

Rubin, A.M., 1995. Propagation of magma-filled cracks. Annu. Rev. Planet. Sci. 23, 287–336.

Sparks, R.S.J., et al., 1998. Magma production and growth of the lava dome of the Soufrière Hills volcano, Montserrat: November 1995 to December 1997. Geophys. Res. Lett. 25, 3421–3424.

Sparks, R.S.J., Young, S.R., 2002. The eruption of Soufrière Hills volcano, Montserrat (1995–1999): overview of scientific results. Mem. Geol. Soc. London 21, 45–69.

Sparks, R.S.J., Baker, L., Brown, R.J., Field, M., Schumacher, J., Stripp, G., Walters, A.L., 2006. Dynamics of kimberlite volcanism. J. Volcanol. Geotherm. Res. 155, 18–48.

Sturton, S., Neuberg, J., 2006. The effects of conduit length and acoustic velocity on conduit resonance: implications for low-frequency events. J. Volcanol. Geotherm. Res. 151 (4), 319–339. doi:10.1016/j.jvolgeores.2005.09.009.

Swanson, D.A., Holcomb, R.T., 1999. Regularities in growth of the Mount St. Helens dacite dome 1980–1986. In: Fink, J.H. (Ed.), Lava flows and domes: emplacement mechanisms and hazards implications. Springer Verlag, Berlin, pp. 3–24.

Troise, C., Pingue, F., De Natale, G., 2003. Coulomb stress changes at calderas: modeling the seismicity at Campi Flegrei (southern Italy). J. Geophys. Res. 108 (B6). doi:10.1029/2002JB002006.

Voight, B., et al., 1999. Magma flow instability and cyclic activity at Soufrière Hills Volcano, Montserrat. Science 283, 1138–1142.

Voight, B., et al., 2006. Unprecedented pressure increase in deep magma reservoir triggered by lava-dome collapse. Geophys. Res. Lett. 33, L03312. doi:10.1029/2005GL024870.

Wadge, G., Mattioli, G.S., Herd, R.A., 2006. Ground deformation at Soufrière Hills volcano, Montserrat during 1998–2000 measured by radar interferometry and GPS. J. Volcanol. Geotherm. Res. 152, 157–173.

Williams, S.N., Self, S., 1983. The October 1902 Plinian eruption of Santa Maria volcano, Guatemala. J. Volcanol. Geotherm. Res. 16, 33–56.

Yokoyama, I., Yamashita, H., Watanabe, H., Okada, H., 1981. Geophysical characteristics of dacite volcanism — 1977–1978 eruption of Usu volcano. J. Volcanol. Geotherm. Res. 9, 335–358.